Engineering Science & Technology
https://ojs.wiserpub.com/index.php/EST/

UNIVERSAL WISER PUBLISHER

Research Article

Build Orientation Dependent Dielectric Properties of 3D Printed PUAR/CuO/Graphite Composite Discs

Bhanu Prakash Bisht[1,2], **Vijaykumar Toutam**[1,2*], **Sanjay R. Dhakate**[1,2]

[1]Academy of Scientific and Innovative Research (AcSIR), CSIR-National Physical Laboratory, Dr. K. S. Krishnan Marg, New Delhi 110012, India
[2]Academy of Scientific and Innovative Research (AcSIR), Ghaziabad, 201002, India
E-mail: toutamvk@nplindia.org

Received: 25 March 2026; **Revised:** 30 April 2026; **Accepted:** 21 May 2026

Abstract: Polyurethane acrylate resin discs with Copper Oxide (CuO) and Graphite fillers of different growth orientations from 0° to 90° are fabricated using Digital Light Processing (DLP) 3D printing technique to study their dielectric properties. Three different composites, Polyurethane Acrylate Resin (PUAR)/CuO (PUA-1), PUAR/CuO/Graphite (PUA-2), and PUAR/Graphite (PUA-3), with 1 wt% total filler concentration, are prepared for the present study. X-Ray Diffraction (XRD) analysis of composites shows peaks, 2θ ~ 20.4° (PUAR), 35.4° and 38.6° (CuO), and 26.4° (graphite). Fourier Transform Infrared (FTIR) analysis reveals intensity reduction of C=O and C=C peaks, while the Raman spectrum shows a shift by 20 ± 5 cm^{-1} in PUA-1, 2, and 3, confirming filler interaction with PUAR and phase modification due to polymer-filler interface. Thermo-gravimetric analysis indicates a strong interaction between the filler and the resin, especially for PUA-3, with degradation in two stages at 320 °C and 430 °C due to hard-and soft-segment decomposition. Capacitance measurements at 100 kHz and 1 MHz indicate a higher dielectric constant for PUA-3 than for PUA-0, which decreases with increasing build orientation and reaches a minimum at 45°. Anisotropy due to the build and filler orientation is studied using space-charge polarization. The equivalent circuit for dependence on build orientation is understood in terms of capacitances due to fillers, represented by a Constant Phase Element (CPE), with both perpendicular and parallel components contributing to the composite disc's capacitance. With an increase in build orientation angle, the interfacial polarization decreases and so capacitance, $CPE_0 >> CPE_x > CPE_{90}$. Finite Element Analysis (FEA) further examines build orientation-dependent filler-resin interaction, and dielectric properties show dependence on both filler morphology and build angle. FEA highlights the role of orientation-dependent space-charge distribution and Maxwell-Wagner-Sillars interfacial polarization, driven by filler morphology and alignment, in governing dielectric anisotropy. FEA corroborates the experimental observations, showing that space-charge accumulation at filler-matrix interfaces is maximal for 0° build orientation, where graphite flakes are perpendicular to the electric field, and minimal for 45°-90°.

Keywords: polyurethane acrylate, build orientation, Digital Light Processing (DLP) 3D printing, dielectric polarization

1. Introduction

Polymer-Matrix Composites (PMCs) with different fillers like metals, semiconductors, and oxides have been

DOI: https://doi.org/10.37256/est.7220269878

broadly studied due to ease of processing and have found several applications in different industries like automobile, aerospace, defense, energy storage, Electromagnetic (EM) shielding, electronics, sensing, and actuation [1]-[3]. However, traditional manufacturing technologies such as injection molding, melt mixing, and solution processing have long imposed limitations on the development of application-specific PMCs. The popularity of 3D Printing (3DP) technology drastically altered the applications of PMCs. 3D printing offers complex geometries and high accuracy with minimal waste, whereas conventional methods fail to deliver [4], [5]. Printing of polymer composites combines the matrix and reinforcement to achieve specific geometries, yielding properties that are not attainable by other techniques. There are different types of 3D printing techniques, depending on the material used and the process [6], [7]. Some of the most common techniques are material extrusion, binder jetting, and stereolithography. Stereolithography, also called Stereolithography/Vat Photopolymerization, is a rapid, maskless, layer-by-layer additive manufacturing method capable of creating complex 3D structures from a polymer resin that can be photocured with Ultraviolet (UV) light [8], [9]. Digital Light Processing (DLP), belonging to the VAT photopolymerization technique, has an edge over other 3DP techniques due to its high resolution, simplicity, and demonstrates the feasibility of adding fillers to the resin during printing for creating PMC with desired electrical and mechanical properties for selective applications [10]-[13].

Due to its extensive use in the electronics industry, the study of PMC's dielectric properties has become very important. Dielectric properties are also studied to understand the effect of filler-polymer interfacial chemistry and the effective permittivity of PMCs [14], [15]. The complex permittivity of polymeric nanocomposites depends on their microstructure, the volume fraction, the shapes and types of components, including the matrix, the fillers, and a possible third phase known as the interphase [16], [17].

Dielectric properties of PMC can be explained with the help of models like the Maxwell-Garnett equation [18], Jaysundere-Smith equation [19], Percolation Model [20], etc. Many formulas have been proposed to predict the dielectric properties of bi-phase materials, such as classical mixing rules and formulas based on the Effective Medium Theory (EMT) and Maxwell-Wagner polarization [21]. Using the Maxwell-Garnett formula, the dielectric properties of the mixture can be calculated from the average electric field over both components. Xu et al. performed Finite Element Analysis (FEA) on unidirectional aramid/epoxy composites and predicted that the dielectric constant decreases with increasing θ between the fibers and the applied field, a purely analytical result [22]. Similarly, Islam et al. simulated dielectric properties of Polymethyl Methacrylate (PMMA) composites with spherical fillers (Si, ZnS, Au, TiO_2, $BaTiO_3$) using COMSOL, showing that space-charge polarization dominates. However, their model assumed perfect filler dispersion and did not consider filler orientation anisotropy [23]. Zazoum studied the dielectric response of low-density polyethylene and TiO_2 using analytical methods to simulate frequency-dependent dielectric response and showed that the nanoparticle interphase affects the composite's final dielectric properties [24].

There are very few studies in the literature on the build orientation-dependent properties of 3D printed structures. Hamzah et al. studied the orientation-dependent electrochemical behavior of 3D-printed ABS/Carbon Black electrodes and found that print orientation significantly influences electrochemical behavior [25]. Yao et al. studied tensile failure strength and separation angle of Polylactic Acid (PLA) specimens for 7 different angles [26]. Hanon et al. studied the tribological characteristics of a DLP 3D-printed graphene/resin composite with different build orientations and demonstrated that surface structure influences the friction coefficient under different print orientations [27]. However, there are no studies that emphasize the dependence of dielectric properties on build orientation during 3D printing and the anisotropy induced by filler orientation in the composite. Photocurable Hyperbranched Polymers (HBPs), such as Polyurethane Acrylate Resin (PUAR), are suitable materials for fabricating polymer composites. PUAR has low viscosity, facilitating easy dispersion of fillers; thus, fillers with different loadings can be added to make polymer composites more easily [11]. Many filler inclusions have been incorporated into PUAR for 3D printing applications, including TiO_2, Al_2O_3, and ZnO, to enhance properties such as dielectric performance, radiation shielding, and optical sensing [28]-[30].

Among various filler materials, Copper Oxide (CuO) and graphite offer promising dielectric characteristics for polymer matrix composites. CuO is a transition-metal oxide known for its high dielectric constant and low dielectric loss, making it an excellent candidate for energy storage applications such as batteries and supercapacitors [31]. Nanoscale CuO particles, in particular, exhibit enhanced dielectric permittivity, and studies have shown that their intrinsic dielectric constant can vary with particle size due to surface and quantum confinement effects.

On the other hand, graphite, a layered allotrope of carbon, has a relative dielectric constant of approximately 11.93,

though this value can vary with factors such as particle size, degree of exfoliation, and surface functionalization [32]. The flake-like morphology of graphite facilitates specific alignment within the resin matrix, potentially influencing interfacial charge accumulation and polarization under an applied electric field [33]. When incorporated into a photocurable resin such as PUAR, the combination of CuO's high permittivity and graphite's anisotropic structure is expected to induce filler alignment during 3D printing. These effects may lead to observable anisotropies in the dielectric response of the printed composite, making CuO and graphite ideal fillers for investigating build-orientation-dependent dielectric properties in 3D printed PUAR composites.

It is hypothesized that, based on the anisotropic morphology of graphite flakes and the layer-by-layer nature of DLP printing, the dielectric response is expected to strongly depend on build orientation due to variation in interfacial polarization and filler alignment. No existing study has combined experimental 3D printing of composites with anisotropic fillers, systematic variation of build orientation, experimental dielectric characterization, and FEA validation of orientation-dependent Maxwell-Wagner-Sillars (MWS) polarization. This work bridges this gap by providing both experimental evidence and simulation support for orientation-dependent dielectric anisotropy in DLP-printed composites.

In this context, the present study aims to systematically investigate the influence of build orientation on the dielectric properties of 3D printed PUAR-based composites. Specifically, this work addresses the following research question: at which build orientation angles (0°, 30°, 45°, 60°, and 90°) do the dielectric constants of PUAR/CuO/graphite composites attain their maximum and minimum values, and what underlying polarization mechanisms govern this orientation-dependent behavior. By combining experimental dielectric measurements with finite-element analysis, the study seeks to elucidate the roles of filler alignment and interfacial polarization in determining the dielectric response.

2. Materials & methods

3D-printed PUAR discs are fabricated using Creality LD-002R, a DLP VAT Photopolymerization Additive manufacturing technique. PUAR clear resin used for 3D printing is procured from Anycubic Technology Co., Ltd. CuO nano-powder of size < 50 nm from Sigma-Aldrich and Graphite powder of particle size 7-11 μm from Alfa-Aesar are used as fillers. Disc-shaped 3D models are printed from three different PUAR composite formulations. PUA-0 disc samples made of pristine resin, PUA-1 samples made from PUAR composite with 1 wt% CuO powder, PUA-2 samples using PUAR composites with CuO and Graphite powder each of 0.5 wt% and PUA-3 samples using PUAR composite with 1 wt% Graphite. All the composites are mixed thoroughly using a vortex stirrer at 2,500 RPM for 15 min, followed by ultrasonication for 10 min to break any soft agglomerates for uniform dispersion of fillers in PUAR. Computer-Aided Design (CAD) software is used to create a 3D model, which is then converted into an STL file and sliced with slicer software for layer-by-layer printing. The dimensions of the disc, layer height, exposure time, and supports are controlled by printing parameters fed to the slicer software. The thickness of the discs is 5 mm and the diameter is 30 mm. The layer height is set to 50 μm, with exposure time kept at 50 sec/layer for the first 8 layers and 8 sec/layer for the remaining layers, for pristine PUAR discs. Whereas, for the PUA-1, PUA-2, and PUA-3, the curing time for the initial layers is optimized to 100 sec/layer, and for the remaining layers, it is 50 sec/layer. The values (100 sec initial, 50 sec subsequent) were determined through trial printing, where incomplete curing (leading to delamination) was observed below 80 sec, and over-curing (bleeding) above 120 sec. In one batch, 10 discs are printed with different orientations of 0°, 30°, 45°, 60°, and 90°. The samples are then cured with 405 nm UV light for 5 min.

X-ray diffraction study of pristine resin and the composite is done using "The Rigaku Miniflex II" with a 2θ scan range of 5 to 60° and a scan resolution of 0.02°. Fourier Transform Infrared (FTIR) spectroscopy of the printed composite is done using the Nicolet iS10 system. Raman spectroscopy of the printed samples is performed using a Renishaw InVia Raman microscope equipped with a 785 nm laser. Dielectric Measurements are done using an Agilent Inductance, Capacitance & Resistance (LCR) meter E4980A at 100 kHz and 1 MHz. The Thermogravimetric Analysis (TGA) studies were conducted using a Mettler Toledo TGA instrument under ambient air conditions, over the temperature range of 40-1,000 °C, with a heating ramp rate of 10 °C per minute.

FEA is performed using the Alternating Current/Direct Current (AC/DC) module of COMSOL Multiphysics

6.2. The matrix material is assigned to the dielectric properties of PUAR, graphite, and CuO fillers with appropriate values for relative permittivity (ε_r) and electrical conductivity (σ) [28], [32], [34]. To simulate the space-charge induced polarization due to 3D printing, along with filler polymer interface due to orientation dependence, impedance mismatch due to layer-by-layer deposition is also introduced. Due to this boundary condition, the electric field distribution depends on the build orientation of 3D-printed samples. The effect of impedance across the layers of 3D-printed samples on the effective dielectric properties of the composite, including space-charge accumulation and electric-field distribution, is studied for different composites and build orientations. The sidewalls of the models are considered as periodic boundary conditions, and an input voltage V_{in} with frequency f was applied to the top electrodes with respect to the bottom being at zero potential.

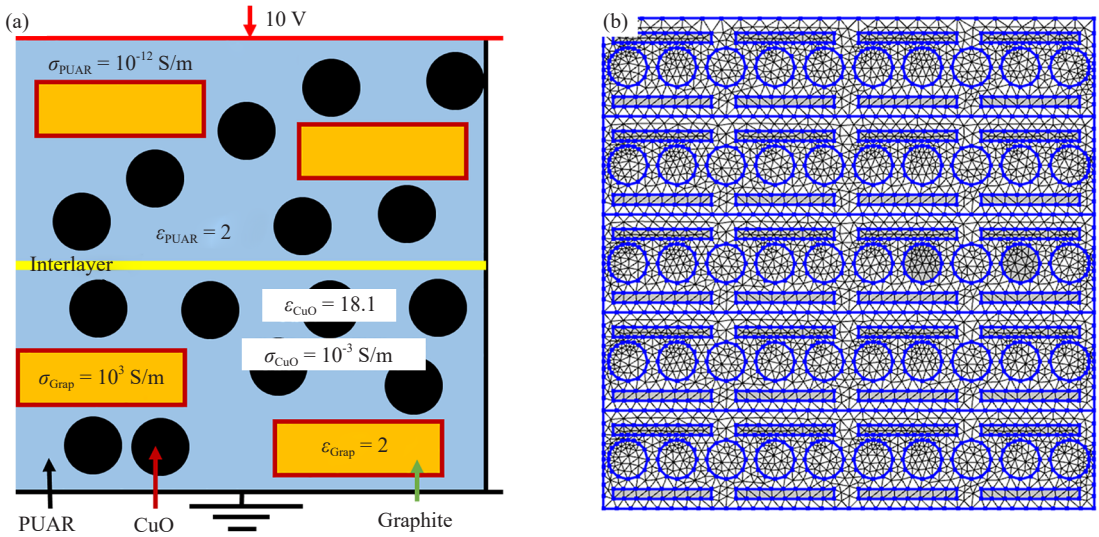

Figure 1. (a) Schematic of the cross-sectional geometry of the Graphite/CuO/PUAR composite disc. (b) Finite element mesh generated using COMSOL Multiphysics, showing the discretization of the composite domain

Figure 1a shows the schematic representation of the cross-sectional profile of the Graphite/CuO/PUAR composite disc, and a similar configuration is used for the finite element analysis. The PUAR matrix is depicted in blue in a 2D rectangular geometry of size 500 nm × 500 nm, which was constructed to represent the cross-sectional image of the PUAR disc composite. Graphite fillers are shown as yellow rectangular inclusions, and CuO nanoparticles are represented as black circular inclusions. The composite is modeled under a parallel-plate capacitor configuration, and the boundary conditions applied included an electric potential ~ 10 V on the upper face of the model and ~ 0 V on the opposite face to simulate a parallel-plate capacitor configuration. The remaining sides were treated as electrically insulated. The frequency-dependent dielectric response was simulated using a harmonic perturbation from 100 kHz to 1 MHz, with a step size of 100 kHz, corresponding to the experimental conditions.

Figure 1b shows the finite element mesh generated for the Graphite/CuO/PUAR dielectric disc. Meshing involves discretizing the geometry into smaller subdomains to enable accurate approximation of the governing physical equations using linear or higher-order polynomial basis functions. This meshing process is fundamental to the finite element method and was performed using COMSOL Multiphysics.

The build orientation-dependent anisotropy was modeled by changing the spatial alignment of fillers within the matrix, mimicking their experimental alignment at 0°, 30°, 45°, 60°, and 90°.

The permittivity of the dielectric discs is calculated via the following equation, which is incorporated into COMSOL. The real (ε') and imaginary (ε'') part of the disc is calculated by following the formulae;

$$\varepsilon' = Re\frac{dI(\omega)}{2i\pi fV_{in}A\varepsilon_0} \tag{1}$$

$$\varepsilon'' = -Im\frac{dI(\omega)}{2i\pi fV_{in}A\varepsilon_0} \tag{2}$$

where A is surface area, d is spacing of parallel plate, $I(\omega)$ is the current flow through the dielectric, ω is the angular frequency, f is the frequency, and V_{in} is the applied potential.

The contact resistance at the electrode-disc interface was modeled as R_c = 100 Ω based on preliminary impedance measurements. The interlayer impedance between printed layers was introduced as a thin boundary layer (thickness = 1 μm) with ε_r = 2.5 and $\sigma = 1 \times 10^{-6}$ S/m, representing the partially cured interface region. Table 1 shows the parameters used in the simulation for PUAR, CuO, and graphite.

Table 1. The conductivity, permittivity and respective reference of PUAR, CuO and graphite

Material	Conductivity (S/m)	Permittivity	Source
PUAR	10E-11	2	[28]
Graphite	3E + 3	11	[32]
CuO	10E-7	18.1	[34]
PUAR intermediate layer	10E-7	--	[35]
CuO/PUAR interface	10E-5	--	[36]

3. Results and discussion

Figure 2 shows the image of PUAR/CuO/Graphite discs with different build orientations, X-Ray Diffraction (XRD), FTIR, and Raman of the PUA-0, PUA-1, PUA-2, and PUA-3 composite discs.

Figure 2a shows images of the disc samples printed with support for each build orientation (0, 30, 45, 60, and 90°) in two batches. The supports are optimized for foot width and density for overhangs, especially for printing samples with build orientation above 45°. Figure 2b shows the samples printed with optimized conditions. The UV light is scattered much more by the fillers in the resin, preventing the printing of discs at higher build orientations (greater than 45°). Further, the support for composites is modified for better printing. The density of supports is increased to 80%, and the contact tip diameter to the disc is kept higher (1.5 mm). In the present study, printing parameters, including support density (80 %) and contact tip diameter (1.5 mm), were optimized to ensure successful fabrication without detachment, visible delamination, or warping, while maintaining dimensional accuracy within ± 0.1 mm.

Figure 2b shows the XRD graphs of PUA-0, PUA-1, PUA-2, and PUA-3, respectively. The XRD pattern of the composite shows characteristic peaks of CuO and Graphite, along with an amorphous peak from the resin. The broad peak at 2θ ~ 20.4° denotes the amorphous phase of cured PUA resin. The characteristic diffraction peaks at 35.4° and 38.6° correspond to the interplanar spacings of the (110) and (111) planes, respectively, indicating the monoclinic structure of CuO NPs. The graphitic peak corresponding to the (002) plane is observed at 26.4° [37].

FTIR spectroscopy is done to study the interaction of the PUAR matrix with CuO and Graphite particle fillers, as shown in Figure 2c. The Peaks at 2,920 and 2,855 cm^{-1} wavenumber correspond to the asymmetric and symmetric stretching vibration of methyl groups (C-H), respectively. A strong band at 1,720 cm^{-1} wavenumber corresponds to the ester carbonyl group (-C=O) of acrylate present in PUAR. A weak band at 1,635 cm^{-1} is attributed to C=C stretching, and the band at 1,110 cm^{-1} is assigned to C-O-C stretching [38]. Upon addition of 1 wt% CuO nanofillers, the intensities of the C=O and C=C bands decrease, indicating interaction between the polymer matrix and CuO NPs, likely due to the

nonavailability of functional groups in PUAR [39]. Further, the addition of graphite suppresses the C-O-C bond and weakens the intensity as observed in PUA-2, and is completely absent for PUA-3, where 1 wt% of graphite is mixed with the PUAR. The interaction of the graphitic carbon through π-electrons with the carboxylic groups reduces the degree of freedom of the polyurethane acrylate C-O bond and is completely absent for PUA-3 [40]. This observation suggests that the graphite filler modifies the PUAR via C-O-C interactions.

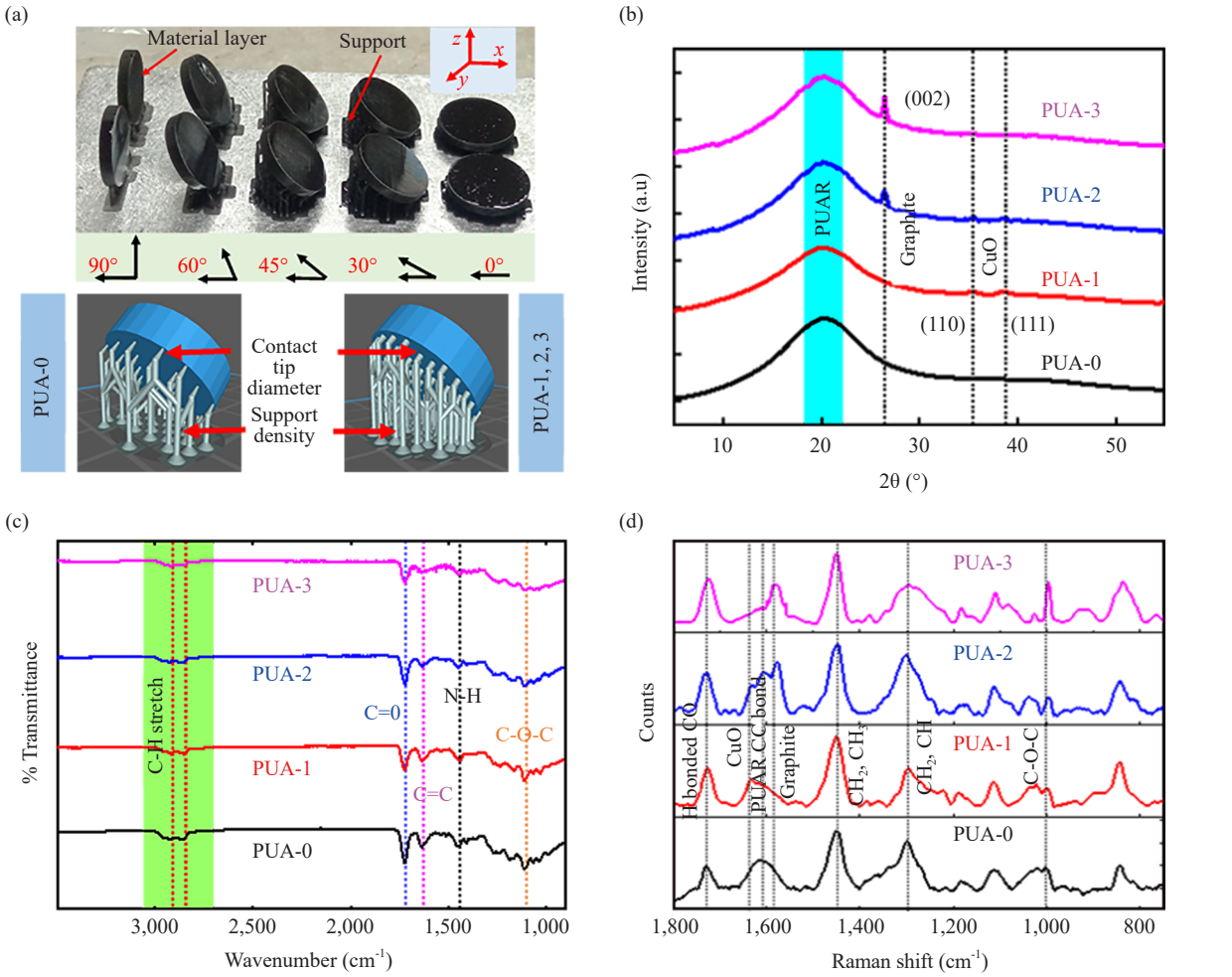

Figure 2. The characterization of the PUAR discs and the discs printed with different orientations. (a) PUAR composite discs printed with different orientations and supports, (b) XRD, (c) FTIR spectra, and (d) Raman spectra of the PUA-0, PUA-1, PUA-2, and PUA-3 composites, respectively

Figure 2d shows Raman spectra of both PUAR and its composites with CuO and Graphite. The signature peak at 1,724 cm^{-1} of PUAR corresponds to the stretching vibration of H-bonded C=O of urethane, and 1,612 cm^{-1} corresponds to the C=C vibration. Graphitic peak is observed at 1,577 cm^{-1}. A broad peak at 1,050 cm^{-1} comprises two subpeaks in PUA-0; one peak is at 999 cm^{-1} and the other at 1,020 cm^{-1}, corresponding to C-O-C and CH vibrational bands, respectively. With the addition of fillers, the peak at 999 cm^{-1} undergoes a red shift and is found to be the maximum for a complete graphite PUAR composite (PUA-3). Graphite flakes have a large surface area and interact with carbonyl groups of PUAR. The addition of Graphite fillers increases the number of interfacial defects. The dipoles induced at the interface of graphite/PUAR make the C-O-C bonds abundant. These bonds are Raman active, and the Raman spectra of PUAR composites show an increase in the intensity of these bands with increasing Graphite filler percentage [41].

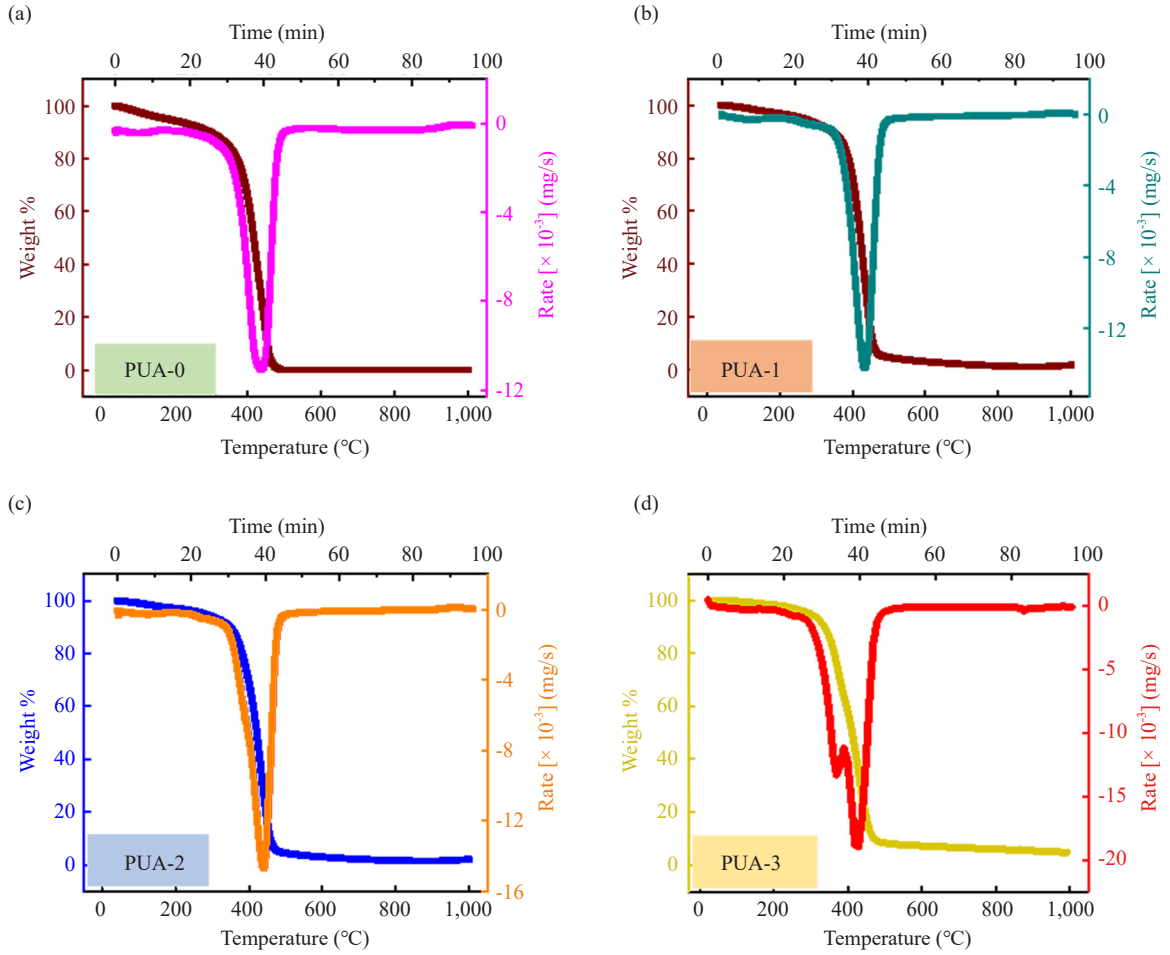

Figure 3. TGA of PUAR and its composite with CuO and Graphite. TGA of (a) pristine PUAR, (b) PUAR with CuO, (c) PUAR with CuO and Graphite, and (d) PUAR with graphite

Figure 3 compares TGA data for PUAR and its composites. Figure 3a-3d shows the temperature-dependent weight loss (left y-axis) and rate of weight loss (right y-axis) of PUA-0, PUA-1, PUA-2, and PUA-3 composites. In PUAR, two different segments are present in the polymer chain. One is the Hard Segment (HS) comprised of isocyanate groups, and the other is the Soft Segment (SS) comprised of polyol groups. Both these segments respond differently to the thermal energy. As a result, the thermal degradation of the PUAR occurs in two stages [42].

As shown in Figure 3, polymer degradation begins at ~ 240 °C due to the dissociation of urethane groups. With the addition of fillers, both CuO and graphite, i.e., for PUA-1 to PUA-3, this degradation temperature goes down to 200 °C. Also, from the gradient of weight loss, the degradation temperature corresponds to the dissociation and decomposition of both hard and soft segments. At lower temperatures, decomposition of the HS occurs, where the dissociation of the urethane from the isocyanate groups takes place, and at higher temperatures, the degradation of the polyol groups occurs, corresponding to the soft segment [43]. From Figure 3a, the decomposition takes place at 433 °C for PUA-0 pristine and is the same for PUA-1 and increases for PUA-2 but reduces for PUA-3. Clearly, the TGA data for the composites suggest that the filler interacts with both the hard and soft segments of PUAR, and, more importantly, that the addition of graphite affects the soft segments, lowering the temperature by 12 °C to 421 °C. Further, the TGA of the PUA-3 composite shows a double-stage decomposition as observed in Figure 3d. The degradation of the hard segment is distinctly present for the PUA-3, suggesting that the graphite is more effective in interacting with PUAR, and the TGA data for PUA-1 show that the addition of CuO has a negligible effect on the decomposition of PUAR. Having established the orientation-dependent dielectric behavior and the filler-matrix interactions through spectroscopic and thermal analyses, we now interpret these findings in the context of Maxwell-Wagner-Sillars polarization theory and the

proposed equivalent circuit model.

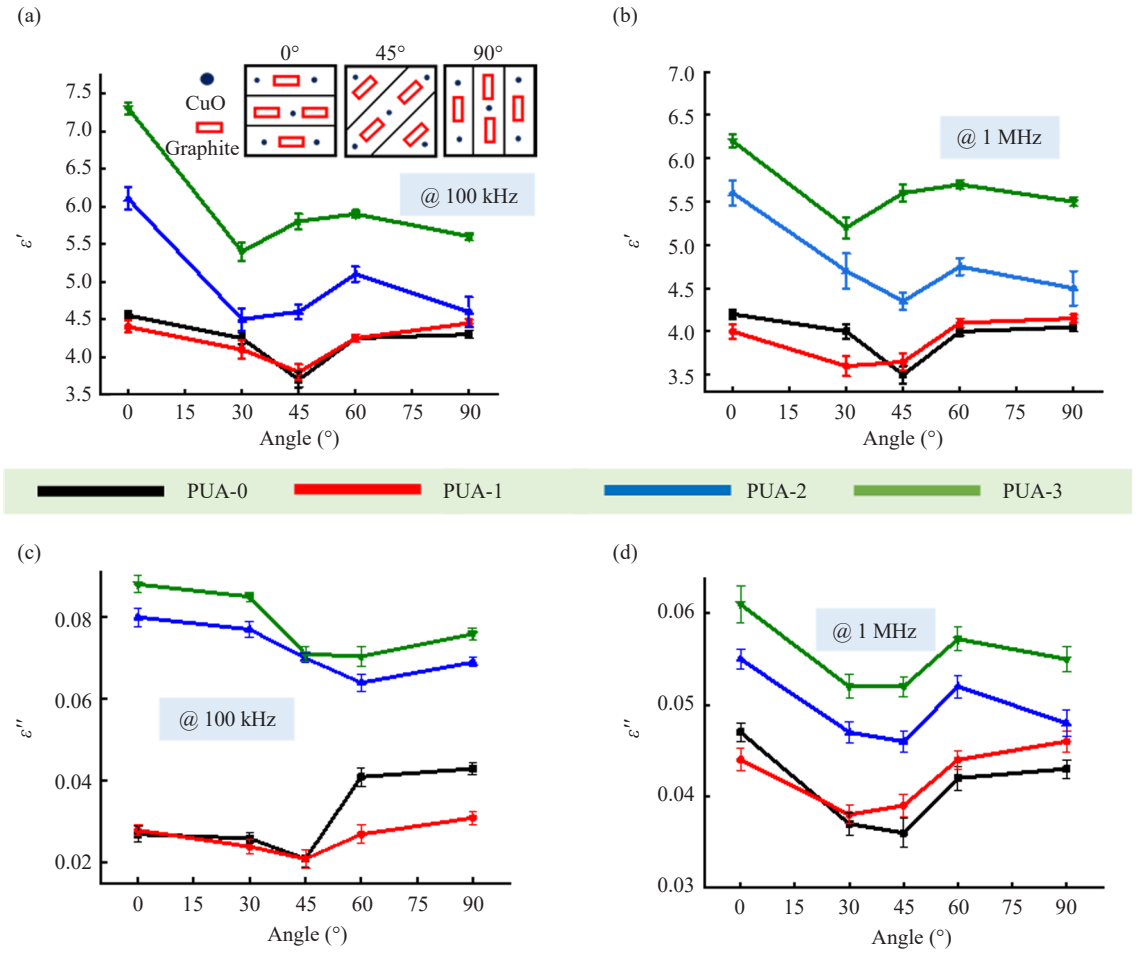

Figure 4. Dielectric measurement of PUA-0, PUA-1, PUA-2, and PUA-3 composites with different orientations (a) Dielectric measurement with frequency of 100 kHz and inset showing dielectric disc with different build orientation (b) Dielectric measurement at 1 MHz frequency (c) Dielectric loss at frequency of 100 kHz and (d) Dielectric loss at frequency of 1 MHz

Figure 4 shows the build-orientation-dependent dielectric behavior of PUAR composites at 100 kHz and 1 MHz.

Figure 4a and 4b show the dielectric behavior of PUA-0, PUA-1, PUA-2, and PUA-3 for different build orientations of 0°, 30°, 45°, 60°, and 90° at a frequency of 100 kHz and 1 MHz, respectively, along with an inset showing a schematic of the filler orientation of dielectric discs for different build orientations. The experimental dielectric constant values of pristine PUAR (PUA-0) are in agreement with a reported value of 3-5 for PUAR [28]. From Figure 4a, it is evident that the dielectric constant of PUAR and its composite is dependent on the build orientation during 3D printing. For all the samples, the dielectric constant behavior shows a decreasing trend with an increasing angle of build orientation. Intriguingly, the minima of the dielectric constant occur between 30 and 45° for all samples. For pristine PUAR (PUA-0), the dependence of dielectric constant is solely from build orientation and is attributed to layer-by-layer deposition during 3D printing. Intermediate exposure of PUAR resin to ambient air during 3D printing results in interface formation across layers, thereby increasing impedance at the interfaces. For a 0° degree build orientation, the impedance mismatch is maximum, and hence the space charge and dielectric constant.

Also, the schematic in Figure 4a shows the filler orientation relative to the build orientation of the 3D-printed samples. With the addition of fillers during layer-by-layer deposition, anisotropy is introduced as they align with the build orientation. For spherical particles like CuO NPs used in 3D printed PUA-1 composite, the anisotropy is negligible

or nil, and, due to low filler percentage, the phase segregation of the particles along the build orientation is ruled out. From the Raman spectra in Figure 2d, it is observed that CuO exhibits a strong peak that suppresses the PUAR peak at 1,612 cm^{-1}. Also, it is known that CuO exhibits increased oxygen deficiency due to its nanoscale dimension and can minimize interfacial stress and suppress dipole formation [44]. Hence, the measured dielectric constant of PUA-1 for 0 and 30° is less compared to the other build orientations, where the interfacial stress is minimized, and is similar for other build orientations, such as PUA-0. When graphite flakes are added to PUAR/CuO composite, the dependence of dielectric constant on the build orientation of 3D printed PUA-2 samples has increased two-fold. Graphite, being electrically conductive and flaky, introduces anisotropy due to its build orientation and increases the interfacial charge density, leading to space-charge-induced dipoles [33]. The dielectric constant of PUA-2 at 100 kHz is ~ 6 at 0° and ~ 4.5 at 90° build orientation, with minima at 30° and 45°. The behavior at 1 MHz for all the PUA samples is similar to that observed at 100 kHz, except that the dielectric constant values have decreased. For 0° build orientation, the dielectric constant of PUA-2 decreased by 0.5 at 1 MHz compared to 100 kHz. This decrease in the dielectric constant with increasing frequency is consistent with a frequency-dependent dielectric constant.

To further understand the effect of graphite loading on the dielectric constant, the PUAR composite with 1 wt% of graphite and no CuO loading is studied to build an orientation-dependent dielectric constant. Figure 4a and 4b show the dielectric-constant behavior of the graphite/PUAR (PUA-3) composite (green color). The behavior of the dielectric constant with build orientation is similar to that of the remaining composites, except that the minima are observed at 30°. Also, the magnitude of the dielectric constant from 0° build orientation has increased with the addition of graphite. For PUA-2, the dielectric constant is 6.1, whereas for PUA-3, the dielectric constant is 7.3, which is 128% more than the dielectric constant of the pristine PUAR. In the Raman spectra, the red shift of the C-O-C peak (999 cm^{-1} → lower wavenumber) correlates with increasing dielectric constant across PUA-0 → PUA-1 → PUA-2 → PUA-3, indicating that filler-induced stress at the polymer interface directly enhances interfacial polarization. It is also evident from TGA that thermal degradation temperature in PUA-3 (421 °C vs. 433 °C for pristine) to increased chain mobility at the graphite-PUAR interface, which enhances dipolar polarization and contributes to the higher dielectric constant ($\varepsilon' = 7.3$). This demonstrates the interaction of graphite with PUAR in generating space charge, as confirmed by FTIR, Raman, and TGA data.

Figures 4c and 4d show the variation of dielectric loss (ε'') for PUA-0, PUA-1, PUA-2, and PUA-3 as a function of build orientation at frequencies of 100 kHz and 1 MHz, respectively.

Figure 4c shows that the dielectric loss of all samples exhibits a noticeable dependence of dielectric loss on build orientation, with a general trend showing a decrease in ε'' from 0° to 30-45°, followed by an increase towards higher orientations. This behavior correlates with the dielectric constant trend and suggests that interfacial polarization and associated charge carrier dynamics are strongly influenced by the orientation-dependent layer interfaces and filler alignment. Among the samples, PUA-2 and PUA-3 show relatively higher dielectric loss compared to PUA-0 and PUA-1, which can be attributed to the presence of graphite flakes. The conductive nature of graphite facilitates charge-carrier movement, leading to increased energy dissipation through interfacial polarization and leakage mechanisms. The minima observed at intermediate orientations (30-45°) indicate reduced charge accumulation and lower interfacial losses, consistent with reduced dielectric constant in this orientation range.

Figure 4d shows the dielectric loss at 1 MHz, the overall dielectric loss values decrease for all samples compared to 100 kHz. This reduction is due to the inability of charge carriers to follow the rapidly alternating electric field, thereby suppressing interfacial polarization effects. However, the orientation-dependent trend persists, indicating that the structural anisotropy introduced during 3D printing continues to influence dielectric behavior even at higher frequencies. The relatively higher dielectric loss in graphite-containing samples (PUA-2 and PUA-3) further confirms the role of conductive fillers in enhancing interfacial polarization and energy dissipation. The 128% increase (from $\varepsilon' \approx 3.2$ for PUA-0 to $\varepsilon' \approx 7.3$ for PUA-3 at 0° orientation) is attributed to MWS interfacial polarization. According to MWS theory, when a conductive filler (graphite, $\sigma \approx 10^3$ S/m) is dispersed in an insulating matrix (PUAR, $\sigma \approx 10^{-10}$ S/m), free charges accumulate at the interface under an applied AC field. The effective permittivity enhancement follows:

$$\varepsilon'_{eff} = \varepsilon'_m + \frac{\left(\varphi_f \varepsilon'_f\right)}{\left(1+\left(\omega_\tau\right)^2\right)} \tag{3}$$

where φ_f is filler volume fraction (≈ 0.01 for 1 wt%), τ is the interfacial relaxation time. For graphite flakes with a high aspect ratio (≈ 10 : 1), τ is substantially longer than for spherical CuO particles, leading to stronger MWS polarization even at identical mass loading. This explains why PUA-3 shows higher ε' than PUA-2, despite both having 1 wt% total filler.

In heterogeneous dielectrics with conducting inclusions in an insulating matrix, charge carriers migrate under an applied field and accumulate at interfaces, where conductivity changes discontinuously. The relaxation time for MWS polarization is given by

$$\tau_{\mathrm{MWS}} = \frac{\varepsilon_0 \left(\varepsilon'_m + \varepsilon'_f\right)}{\left(\sigma_m + \sigma_f\right)} \tag{4}$$

For PUAR ($\sigma_m \approx 10^{-10}$ S/m) and graphite ($\sigma_f \approx 10^{3}$ S/m), $\tau_{\mathrm{MWS}} \approx 10^{-5}$-$10^{-4}$ s, corresponding to characteristic frequencies of 10^{4}-10^{5} Hz our measurement range (10^{5}-10^{6} Hz) captures the tail of this relaxation. For a graphite flake with aspect ratio α = l/d (length/diameter), the effective depolarization factor N along the long axis is approximately $(1/\alpha^2)$ ln(α). When the electric field is perpendicular to the flake (0° orientation), N is minimized, maximizing the local field enhancement and MWS polarization. When the field is parallel (90° orientation), N is maximized, suppressing polarization. This theoretical framework now explicitly supports our experimental observations.

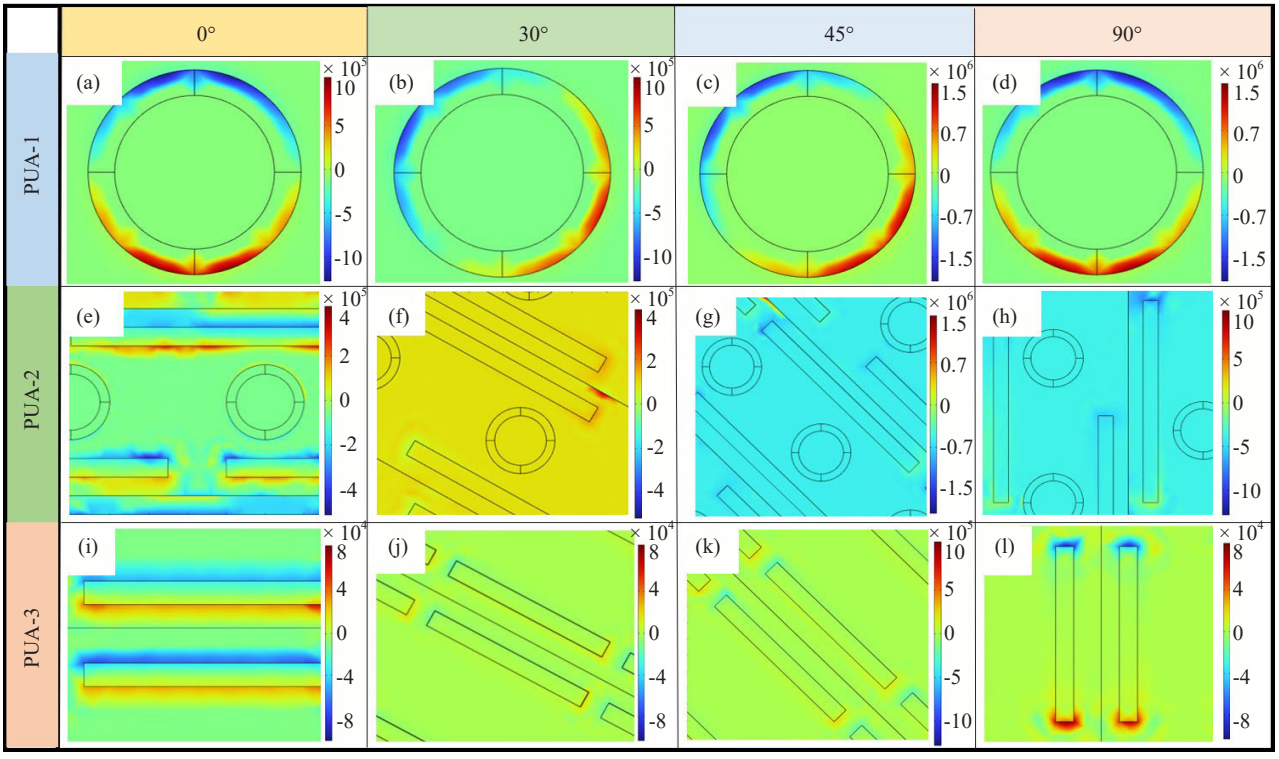

Figure 5. Space charge accumulation of nanoparticle and graphite flakes, (a-d) CuO NPs in PUA-1 composite, (e-h) shows the CuO NPs and graphite flakes in PUA-2 composite, and (i-l) shows the Graphite flakes in PUA-3 composite under 0, 30, 45 and 90° orientation, respectively

A finite element analysis is performed to investigate the dependence of the dielectric constant on build orientation for pristine PUAR and its composites with CuO and CuO/Graphite as fillers in COMSOL Multiphysics using the AC/DC module. Figure 5 shows the finite element analysis of the section of PUA-1 consisting of CuO NPs (circular) as a filler (Figure 5a-d) and PUA-2 consisting of CuO NPs and Graphite flakes (rectangular) (Figure 5e-h), and PUA-3 consisting

only of Graphite flakes (rectangular) (Figure 5i-l) for different build orientations of 0, 30, 45, and 90° respectively.

From Figure 5a-d it is evident that the space charge accumulation at the interface of CuO NPs and polymer matrix is dependent on the build orientation angle. As the CuO NPs are modeled as spherical particles, polarization depends on the applied electric field orientation but shows no anisotropy due to particle shape. Hence, the behavior agrees with that of the PUA-1 composite. Figure 5e-h simulates the anisotropy of the graphite flakes in the PUA-2 sample; the dependence of the dielectric constant on the orientation of the graphite flakes is evident through the space charge distribution around these flakes. This is due to increases in double-layer capacitance, and the voltage required for charge injection is higher due to interface trapping and Maxwell-Wagner-Sillars polarization. The space-charge distribution is maximum for 0° orientation as the electric field is normal to the plane of the flakes. For 90° build orientation, it is minimum and intermediate for 30° and 45°.

Figure 5i-l shows the simulated images of the PUA-3 composite in which the graphite flakes are aligned with the build direction, and the polarization is mainly on the faces of the graphite flakes. A similar observation in PUA-3 composites through space charge distribution around these flakes is observed in PUA-3. As the graphite composition is larger compared to PUA-2, PUA-3 shows the highest dielectric constant.

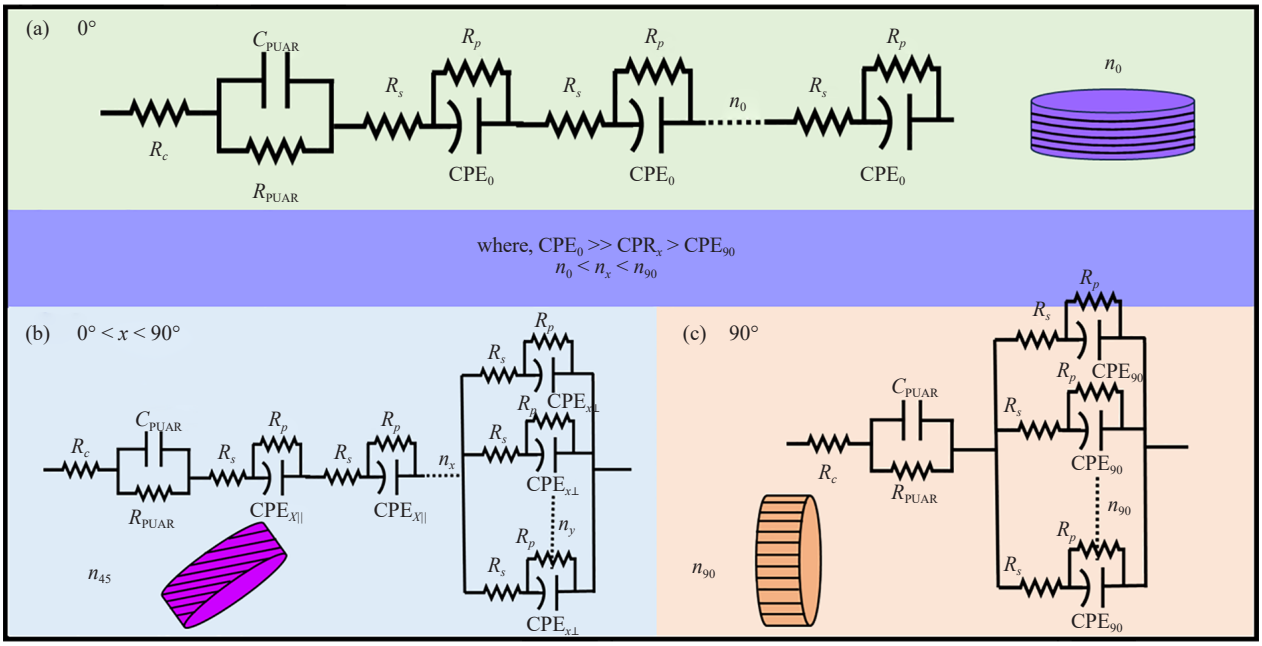

Figure 6. Equivalent circuit model for (a) 0°, (b) $0° < x < 90°$, and (c) 90° build orientation of Graphite/CuO/PUAR composite disc, along with the discs showing layers in printing direction, respectively

Figure 6 of the Graphite/CuO/PUAR disc, where n_0, n_{45}, and n_{90} are the number of layers in the discs with 0°, 45°, and 90° orientation discs.

Figure 6a shows the equivalent circuit model for the resultant capacitance of PUAR composite discs with 0° build orientation, where the printed layers are aligned horizontally, and the fillers (CuO and graphite) are oriented perpendicular to the electric field. In this configuration, the electric field discontinuity and fringe field effect are large due to the large surface area of graphite flakes oriented perpendicular to the applied field. The large-area interaction of the electric field generates strong transverse interfacial polarization at the surface of these fillers. This enhances the polarization capability and increases the capacitance of the Graphite/CuO/PUAR disc. The capacitance due to interfacial polarization is modeled as a Constant Phase Element (CPE), which accounts for the non-ideal capacitive behavior arising from fringe-field-induced interfacial polarization, especially around the graphite flakes. The equivalent circuit includes a contact resistance (R_c) at the electrode-disc interface, followed by an Resistance Capacitance (RC) pair representing the bulk PUAR matrix behavior (R_{PUAR} and C_{PUAR}) and the capacitance due to fillers. Even though the

impedance mismatch is built into the layered structure due to PUAR, its effect on determining the final capacitance is minimal compared to the impedance mismatch and charge polarization at the interface between PUAR and graphite. Hence, the capacitance due to the entire PUAR matrix, regardless of the build orientation, is represented as a constant. The sole dependence of capacitance is idealized due to the filler orientation during 3D printing. As CuO is spherical and has a high dielectric constant ~ 18, the isotropic nature has minimal charge polarization at the interface compared to graphite flakes. The constant phase element denoted by CPE_0 is solely due to graphite, and the layered deposition makes this contribution effective for the serial configuration. Each unit consists of a CPE_0, a parallel resistance (R_p), and a series resistance (R_s), where R_p accounts for localized leakage or conduction along the filler-polymer interface, while R_s offers charge transport resistance across the conduction path either due to filler agglomeration, layer boundaries, or disrupted polymer segments. Based on the number of layers n_0 and CPE being large, the effective contribution from CPE_0 is large and is the deciding factor in the capacitance for 0° build orientation of the PUAR composite disc. For any other angle between 0 and 90°, the CPE element has contributions from both components of parallel ($CPE_{X||}$) and perpendicular ($CPE_{X\perp}$), as represented in Figure 6b. In this configuration of build orientation $0° < x < 90°$, the CPE due to normal add up in a serial configuration, and the CPE due to parallel add up in a parallel configuration. As the angle of orientation increases, the normal component decreases and the parallel component increases, as shown in Figure 6c. As the surface area of the flakes perpendicular to the electric field decreases with an increase in build orientation, the $CPE_{X||}$ is smaller, and the resultant capacitance shows a decreasing trend with an increase in build orientation up to 45°. Further increase in build orientation, the number of layers for printing increases, and for 90°, the layer number is maximum. i.e., $n_0 << n_{45} << n_{90}$. As the layer-by-layer deposition packs more particles due to more layers and the resultant capacitance is solely due to a parallel combination, the electric field flows along the layer plane, leading to minimal interfacial polarization across the printed interfaces. The capacitance for 90° build orientation effectively matches or slightly exceeds that for 30 to 45° build orientation, where the minimum capacitance is observed. Hence, the equivalent circuit for dependence on build orientation introduces CPE both due to perpendicular and parallel components and contributes to the effective capacitance of the composite disc. Graphite, due to its metallic nature, induces strong interfacial polarization and is a major contributor to the capacitance dependence on build orientation. This work addresses the gap in understanding how build orientation in DLP 3D printing influences dielectric behavior in PUAR polymer composites. It demonstrates that build orientation dependent modulates dielectric response, with a consistent minimum at 30°-45°, and establishes the role of anisotropic filler alignment and interfacial (Maxwell-Wagner-Sillars) polarization, supported by experimental observations and finite element analysis.

4. Limitations and future perspectives

1. Direct quantification of density, internal defects, and interlayer bonding was not performed in this study. Future work will focus on detailed microstructural characterization using SEM, such as cross-sectional imaging, to further correlate structural quality with dielectric properties.

2. The present study focuses on a representative filler concentration (1 wt%) and a selected frequency range (100 kHz-1 MHz) to capture the dominant orientation-dependent dielectric behavior. While this provides clear insight into interfacial polarization mechanisms, extending it to broader compositions, frequency ranges, and more detailed microstructural analysis would add depth. These aspects will be explored in future work.

5. Conclusion

PUAR and PUAR composite discs are 3D printed using the DLP technique. The dependence of dielectric properties on build orientation during 3D printing is studied for different angles. The interaction of the interlayer and filler particle is studied by FTIR, Raman spectroscopy, and XRD. Further, the dielectric properties and the interactions of the filler particles, CuO and graphite, with PUAR are studied in parallel-plate capacitance mode at different frequencies. The interfacial effects induced by intermittent layer-by-layer deposition are studied to determine the dependence of dielectric properties on build orientation. Also, the effect of filler particle-induced polarization and anisotropy arising from layer-

by-layer deposition on the dielectric properties is studied. The study confirms that the dielectric constant dependence is due to the build orientation and that the minimum occurs at 30° and 45° for all samples. Also, the anisotropy of the fillers like graphite, increases the dielectric constant of the composite due to Maxwell-Wagner-Sillars polarization. The study is further augmented by finite element analysis of the composite models, which depict the anisotropy induced by build orientation-dependent space-charge polarization.

Acknowledgements

Mr. Bhanu Prakash Bisht acknowledges the Council of Scientific and Industrial Research (CSIR) & Academy of Scientific and Innovative Research (AcSIR) for fellowship and academic support. Dr. Vijaykumar Toutam acknowledges CSIR for financial support under the Lab Project (Project No. OLP-230432) and in-house R&D support. We acknowledge Dr. Satish Singh for the preliminary dielectric measurement.

Conflict of interest

The authors declared that there is no competing interest involved.

Reference

[1] R. Hsissou, R. Seghiri, Z. Benzekri, M. Hilali, M. Rafik, and A. Elharfi, "Polymer composite materials: A comprehensive review," *Composite Structures*, vol. 262, pp. 113640, 2021.
[2] S. Sajan and D. Philip Selvaraj, "A review on polymer matrix composite materials and their applications," *Materials Today: Proceedings*, vol. 47, pp. 5493-5498, 2021.
[3] K. Czech, R. Oliwa, D. Krajewski, K. Bulanda, M. Oleksy, and G. Budzik, "Hybrid polymer composites used in the arms industry: A review," *Materials*, vol. 14, no. 11, pp. 3047, 2021.
[4] M. Jayakrishna, M. Vijay, and B. Khan, "An overview of extensive analysis of 3D printing applications in the manufacturing sector," *Journal of Engineering*, vol. 2023, no. 1, pp. 7465737, 2023.
[5] J. López-Barroso, C. G. Flores-Hernández, A. L. Martínez-Hernández, G. Martínez-Barrera, and C. Velasco-Santos, "Additive manufacturing for complex geometries in polymer composites," in *Advanced Composites*, S. J. Ikhmayies, Ed. Cham, Switzerland: Springer Nature Switzerland, 2024, pp. 121-186.
[6] A. Jandyal, I. Chaturvedi, I. Wazir, A. Raina, and M. I. Ul Haq, "3D printing-A review of processes, materials and applications in industry 4.0," *Sustainable Operations and Computers*, vol. 3, pp. 33-42, 2022.
[7] D. Srinivasan, M. Meignanamoorthy, M. Ravichandran, V. Mohanavel, S. V. Alagarsamy, C. Chanakyan, S. Sakthivelu, A. Karthick, T. Ram Prabhu, and S. Rajkumar, "3D printing manufacturing techniques, materials, and applications: An overview," *Advances in Materials Science and Engineering*, vol. 2021, pp. 5756563, 2021.
[8] S. Subedi, S. Liu, W. Wang, S. M. A. N. Shovon, X. Chen, and H. O. T. Ware, "Multi-material vat photopolymerization 3D printing: A review of mechanisms and applications," *npj Advanced Manufacturing*, vol. 1, no. 1, pp. 9, 2024.
[9] J. Feng, J. Fu, Z. Lin, C. Shang, and B. Li, "A review of the design methods of complex topology structures for 3D printing," *Visual Computing for Industry, Biomedicine, and Art*, vol. 1, no. 1, pp. 5, 2018.
[10] S. Park, W. Shou, L. Makatura, W. Matusik, and K. Fu, "3D printing of polymer composites: Materials, processes, and applications," *Matter*, vol. 5, no. 1, pp. 43-76, 2022.
[11] A. Al Rashid, W. Ahmed, M. Y. Khalid, and M. Koç, "Vat photopolymerization of polymers and polymer composites: Processes and applications," *Additive Manufacturing*, vol. 47, pp. 102279, 2021.
[12] T. Ma, Y. Zhang, K. Ruan, H. Guo, M. He, X. Shi, Y. Guo, J. Kong, and J. Gu, "Advances in 3D printing for polymer composites: A review," *InfoMat*, vol. 6, no. 6, pp. e12568, 2024.
[13] M. Alshihabi and M. Y. Kayacan, "Enhancing electrical and magnetic properties in SLA 3D printed resin composites with nano MWCNT, TiN, and c-BN powders," *Polymers for Advanced Technologies*, vol. 36, no. 2, pp. e70109, 2025.
[14] R. Quader, L. K. Narayanan, and E. B. Caldona, "Dielectric characterization of fiber-and nanofiller-reinforced

polymeric materials," *Journal of Applied Polymer Science*, vol. 141, no. 19, pp. e55362, 2024.
[15] G. Jian, L. Feng, Y. Du, N. Yang, S. Zhu, R. Dong, and Y. Jiao, "Dielectric properties of a linear polymer-matrix composite filled with aligned Ag@$BaTiO_3$ flakes," *Journal of Alloys and Compounds*, vol. 947, pp. 169477, 2023.
[16] Q. Wang, J. Che, W. Wu, Z. Hu, X. Liu, T. Ren, Y. Chen, and J. Zhang, "Contributing factors of dielectric properties for polymer matrix composites," *Polymers*, vol. 15, no. 3, pp. 590, 2023.
[17] P. Gupta, E. Ruzicka, B. C. Benicewicz, R. Sundararaman, and L. S. Schadler, "Dielectric properties of polymer nanocomposite interphases using electrostatic force microscopy and machine learning," *ACS Applied Electronic Materials*, vol. 5, no. 2, pp. 794-802, 2023.
[18] V. A. Markel, "Introduction to the Maxwell Garnett approximation: Tutorial," *Journal of the Optical Society of America A*, vol. 33, no. 7, pp. 1244-1256, 2016.
[19] N. Jayasundere and B. V. Smith, "Dielectric constant for binary piezoelectric 0-3 composites," *Journal of Applied Physics*, vol. 73, no. 5, pp. 2462-2466, 1993.
[20] Z. Wang, J. Zhang, and G. J. Weng, "Modeling the percolation behavior of conductive particles/insulating polymer-based composites with equivalent circuit of resistance," *Polymer*, vol. 324, pp. 128262, 2025.
[21] T. T. N. Vu, G. Teyssedre, S. Le Roy, and C. Laurent, "Maxwell-Wagner effect in multi-layered dielectrics: Interfacial charge measurement and modelling," *Technologies*, vol. 5, no. 2, pp. 27, 2017.
[22] X. Xu, B. Zhang, K. Liu, D. Liu, M. Bai, and Y. Li, "Finite element simulation and analysis of the dielectric properties of unidirectional aramid/epoxy composites," *Polymer Composites*, vol. 39, no. S4, pp. E2226-E2233, 2018.
[23] M. D. Islam, S. Liu, D. Choi, Z. Guo, and J. E. Ryu, "Physics-based computational method predicting the dielectric properties of polymer nanocomposites," *Applied Composite Materials*, vol. 29, no. 4, pp. 1579-1595, 2022.
[24] B. Zazoum, "Hybrid analytical finite element method for dielectric response of PE/TiO_2 nanodielectric materials," *Materials Research Express*, vol. 7, no. 7, pp. 1-10, 2020.
[25] H. H. Bin Hamzah, O. Keattch, D. Covill, and B. A. Patel, "The effects of printing orientation on the electrochemical behaviour of 3D printed acrylonitrile butadiene styrene (ABS)/carbon black electrodes," *Scientific Reports*, vol. 8, no. 1, pp. 1-8, 2018.
[26] T. Yao, J. Ye, Z. Deng, K. Zhang, Y. Ma, and H. Ouyang, "Tensile failure strength and separation angle of FDM 3D printing PLA material: Experimental and theoretical analyses," *Composites Part B: Engineering*, vol. 188, pp. 107894, 2020.
[27] M. M. Hanon, A. Ghaly, L. Zsidai, and S. Klébert, "Tribological characteristics of digital light processing (DLP) 3D printed graphene/resin composite: Influence of graphene presence and process settings," *Materials and Design*, vol. 218, pp. 110718, 2022.
[28] C. Mendes-Felipe, J. C. Barbosa, S. Gonçalves, N. Pereira, C. M. Costa, J. L. Vilas-Vilela, and S. Lanceros-Mendez, "High dielectric constant UV curable polyurethane acrylate/indium tin oxide composites for capacitive sensing," *Composites Science and Technology*, vol. 199, pp. 108363, 2020.
[29] Y. Kavun, A. Acikgoz, and G. Demircan, "DLP 3D printing of Al_2O_3 and Bi_2O_3 reinforced photopolymer composites: Radiation shielding and mechanical properties," *Ceramics International*, vol. 51, no. 17, pp. 23289-23301, 2025.
[30] B. P. Bisht, V. Toutam, S. R. Dhakate, K. M. Subhedar, S. Srivastava, A. Yadav, and G. Gupta, "3D printed ZnO-Polyurethane acrylate resin composite for wide spectral photo response optical detectors," *Sensors and Actuators A: Physical*, vol. 351, pp. 114165, 2023.
[31] C. Gherasim, M. Asandulesa, N. Fifere, F. Doroftei, D. Tîmpu, and A. Airinei, "Structural, optical and dielectric properties of some nanocomposites derived from copper oxide nanoparticles embedded in poly(vinylpyrrolidone) matrix," *Nanomaterials*, vol. 14, no. 9, pp. 759, 2024.
[32] E. Gümüş, M. Yağımlı, and E. Arca, "Investigation of the dielectric properties of graphite and carbon black-filled composites as electromagnetic interference shielding coatings," *Applied Sciences*, vol. 13, no. 15, pp. 8893, 2023.
[33] G. Chen, H. Wang, and W. Zhao, "Fabrication of highly ordered polymer/graphite flake composite with eminent anisotropic electrical property," *Polymers for Advanced Technologies*, vol. 19, no. 8, pp. 1113-1117, 2008.
[34] T. Ghabara, V. Crasta, R. Bairy, and P. C. R. Kumar, "Dielectric, photoluminescence, thermal and mechanical properties of CuO nanoparticles filled polyvinyl alcohol/polyvinyl pyrrolidone blends for high frequency device applications," *ECS Journal of Solid State Science and Technology*, vol. 13, no. 11, pp. 113014, 2024.
[35] M. Feng, Y. Feng, T. Zhang, J. Li, Q. Chen, Q. Chi, and Q. Lei, "Recent advances in multilayer-structure dielectrics for energy storage application," *Advanced Science*, vol. 8, no. 23, pp. 2102221, 2021.
[36] J. Shao, L. Zhou, Y. Chen, X. Liu, and M. Ji, "Model-based dielectric constant estimation of polymeric

nanocomposite," *Polymers*, vol. 14, no. 6, pp. 1121, 2022.
[37] Z. Zhou, W. G. Bouwman, H. Schut, and C. Pappas, "Interpretation of X-ray diffraction patterns of (nuclear) graphite," *Carbon*, vol. 69, pp. 17-24, 2014.
[38] A. Madhi, B. Shirkavand Hadavand, and A. Amoozadeh, "UV-curable urethane acrylate zirconium oxide nanocomposites: Synthesis, study on viscoelastic properties and thermal behavior," *Journal of Composite Materials*, vol. 52, no. 21, pp. 2973-2982, 2018.
[39] S. El-Sayed and A. M. E. Sayed, "Preparation and characterization of CuO/Co_3O_4/poly(methyl methacrylate) nanocomposites for optical and dielectric applications," *Journal of Materials Science: Materials in Electronics*, vol. 32, no. 10, pp. 13719-13737, 2021.
[40] E. M. Pérez and N. Martín, "π-π interactions in carbon nanostructures," *Chemical Society Reviews*, vol. 44, no. 18, pp. 6425-6433, 2015.
[41] M. Strankowski, D. Włodarczyk, Ł. Piszczyk, and J. Strankowska, "Polyurethane nanocomposites containing reduced graphene oxide, FTIR, Raman, and XRD studies," *Journal of Spectroscopy*, vol. 2016, no. 1, pp. 7520741, 2016.
[42] S. M. Cruz and J. C. Viana, "Melt blending and characterization of carbon nanoparticles-filled thermoplastic polyurethane elastomers," *Sage Journal*s, vol. 47, no. 7, pp. 647-665, 2014.
[43] I. Ristić, S. Cakić, N. Vukić, V. Teofilović, J. Tanasić, and B. Pilić, "The influence of soft segment structure on the properties of polyurethanes," *Polymers*, vol. 15, no. 18, pp. 3755, 2023.
[44] L. Li, G. Chen, H. Zheng, W. Meng, S. Jia, L. Zhao, P. Zhao, Y. Zhang, S. Huang, T. Huang, et al., "Room-temperature oxygen vacancy migration induced reversible phase transformation during the anelastic deformation in CuO," *Nature Communications*, vol. 12, no. 1, pp. 3863, 2021.